IEEE Access
Multidisciplinary | Rapid Review | Open Access Journal

Received May 14, 2019, accepted May 28, 2019, date of publication June 19, 2019, date of current version July 8, 2019.

Digital Object Identifier 10.1109/ACCESS.2019.2923711

Two Phase Dual-Stator Axial-Flux PM BLDC Motor With Ironless Rotor Using Only-Pull Drive Technique

TANVEER YAZDAN[1], SHAHID ATIQ[2], BYUNG-IL KWON[3], (Senior Member, IEEE), NOMAN BALOCH[3], AND JUNG-WOO KWON[3]

[1]Electrical Engineering Department, The University of Lahore, Lahore 54000, Pakistan
[2]Electrical Engineering Department, Khwaja Fareed University of Engineering & Information Technology, Rahim Yar Khan 64200, Pakistan
[3]Electronic Systems Engineering Department, Hanyang University, Ansan 15588, South Korea

Corresponding author: Byung-Il Kwon (bikwon@hanyang.ac.kr)

This work was supported by the Korea Institute of Energy Technology Evaluation and Planning (KETEP) and the Ministry of Trade, Industry & Energy (MOTIE) of the Republic of Korea (No. 20174030201780), and in part by the BK21PLUS Program through the National Research Foundation of Korea within the Ministry of Education.

ABSTRACT This paper proposes a two-phase dual-stator axial-flux permanent magnet brushless dc motor with an ironless rotor for higher torque per magnet volume using the only-pull drive technique. The advantage of the ironless rotor is that it reduces magnet volume by providing an effective flux linkage, while the only-pull drive technique, which involves only the pull process, benefits from the use of thin magnets that do not experience the irreversible demagnetization. The axial-flux configuration of the proposed dual-stator motor was adopted because of its capability of achieving the desired trapezoidal back electromotive force that maximizes the advantages of the only-pull drive technique. The thin magnets were fixed on the ironless rotor using a non-magnetic structure, and the stator was particularly designed to implement the only-pull drive technique. The performance of the motor was analyzed in terms of torque per magnet volume using the finite element analysis and validated by the experimental results.

INDEX TERMS Dual-stator motor, finite element analysis, ironless rotor, only-pull drive technique, permanent magnet motor, torque per magnet volume, two phase motor.

NOMENCLATURE

B	flux density
B_r	residual flux density
E	phase back-EMF
g	airgap length
H	coercivity or field intensity
i	phase current
ϕ	flux
θ	angular position

I. INTRODUCTION

Due to their high-performance characteristics such as higher torque density, low maintenance cost, and high reliability, brushless permanent magnet (PM) motors have been widely used in various industrial automation processes including aerospace, traction, and medical applications. However, because of their high cost and limited resources, the effective utilization of PMs for higher torque density has become a challenge for PM motors. To improve the torque density, single rotor PM motors with dual-stator have recently been studied [1]–[5]. The topology of dual-stator PM motors, including the alignment of the stators and the design of each stator, and the rotor, significantly affects torque performance. Aligned stators produce higher torque density compared to the unaligned stators that produce lower torque ripples [6], [7]. Unaligned stators are typically not preferred because of an imbalanced axial force, which is responsible for vibration and noise, and an asymmetrical armature reaction, which is responsible for irreversible demagnetization.

Considering the stator design, dual-stator PM motors contain an equal slot number to improve the torque density, this includes a sandwiched iron core rotor between the two stators [8]–[9]. A rotor with two layers of magnets on both sides of the iron core was constructed to reduce the iron core material. Enhanced torque density was achieved

The associate editor coordinating the review of this manuscript and approving it for publication was Christopher H. T. Lee.

compared to a surface PM motor with one stator and one rotor. A dual-stator topology with a different slot number on the stators and a sandwiched iron core rotor to improve the torque density was presented in [10]. However, a significant amount of the magnet was utilized, causing a reduced torque per magnet volume, making these motors expensive; furthermore, the iron core rotor caused an increase in additional iron losses.

Alternatively, an attempt was made in [11] using a PM rotor to improve the torque per magnet volume and reduce the cost. A dual-stator machine with and without an iron core PM rotor was also presented in [12]. The motor with an ironless rotor had superior power capacity and reduced cogging torque and torque ripples compared to the iron core motor. However, the torque per magnet volume was not significantly improved in this ironless motor because an equal amount of magnet was utilized at almost the same cost instead of thin magnets. Compared to an ironless rotor, an iron core rotor can be subject to saturation because of the higher currents in the windings and the considerable size of the magnet. This saturation can become a source of asymmetric flux distribution as well as a heat production that drives the operating point of the magnets toward or below the knee point on the BH curve [13]–[15].

PM motors typically operate in both the magnetizing (pull) and demagnetizing (push) processes on the recoil line of the BH curve. During the push process, thin magnets are easily demagnetized, and the operating point of the magnets drops on the BH curve because of the demagnetizing fields. These fields act against the permeance of the magnets and can result in the irreversible loss of magnetism under high starting current or winding faults [16], [17]. Demagnetization can cause detrimental effects, such as a lower magnetic flux density, reduction of back electromotive force (EMF), poor electromagnetic torque, and low efficiency [18].

Due to their high susceptibility to demagnetization, thin magnets are typically not utilized in PM motors. To overcome the risk of demagnetization, either thicker magnets are utilized [19], [20] or the impact of the demagnetizing fields is constrained [21]. Thicker magnets contribute significantly to a higher motor cost. Considering the cost factor, demagnetizing fields are commonly constrained either by rotor [22] or stator design. Rotor design focuses on increasing the magnetic reluctances against the demagnetizing fields arising from the stator magneto-motiveforce (MMF) [23], [24]. Stator design addresses the electrical and physical isolation of the stator phases using fractional-slot concentrated windings in fault-tolerant configurations [25], [26]. However, these design considerations add complexity to the structure and require considerable effort and design practice.

Despite significant research on PM motors, the utilization of thin magnets, considering the torque per magnet volume, and their protection against irreversible demagnetization have received minimal attention. Recently, an Only-Pull drive technique was presented in [27] to protect thin magnets against irreversible demagnetization, and this

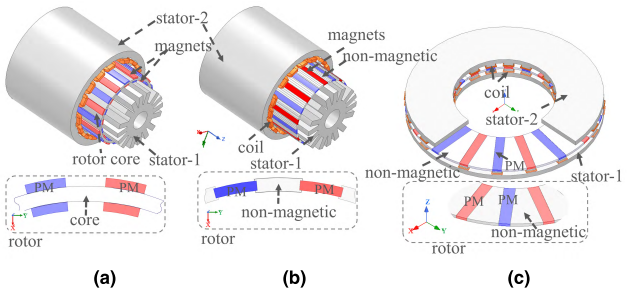

FIGURE 1. Topologies of two phase dual-stators PM motors, (a) DSRF motor, (b) ironless DSRF motor, (c) proposed ironless DSAF motor.

was investigated for a two phase motor. This driving technique requires a unique motor design for implementation and prefers a trapezoidal back-EMF waveform. Compared to a radial-flux motor, an axial-flux motor was found to be useful in producing the desired back-EMF waveform [28]. However, motors with one-stator and one-rotor require a substantial amount of magnet volume, which limits the torque per magnet volume. Furthermore, the iron core material in the motors adds to the rotor iron losses. Design approaches, which improve the torque per magnet volume in these motors while maintaining reliable operation are limited because of the above-mentioned weaknesses.

In this paper, to overcome the problem of low torque per magnet volume, a two phase dual-stator axial-flux (DSAF) PM motor with an ironless rotor driven by the Only-Pull drive technique is proposed. The advantage of this ironless rotor is the reduction of magnet volume by providing an effective flux linkage in both stators with equal slot number. The Only-Pull drive technique involves only a specific region of the flux linkage, i.e., the pull process, and uses a current excitation control to produce the output torque and eliminate the risk of demagnetization. The performance of the proposed ironless DSAF motor is compared in terms of torque per magnet volume with that of an iron core dual-stator radial-flux (DSRF) and an ironless DSRF motor. First, the topologies of the motors are presented. The operating principles of these motors are explained by phenomena of both the flux linkage under no-load and current control under load conditions. The design concept is also presented. Secondly, the results using finite element analysis (FEA) are explored to confirm the topology and design of the proposed ironless DSAF motor. Thirdly, a prototype of the proposed ironless axial-flux motor is built and tested, and complete experimental results are provided. Finally, the conclusions of this research are presented.

II. TOPOLOGIES, OPERATING PRINCIPLES, AND DESIGN CONCEPT

A. TOPOLOGIES

Fig. 1 displays the topologies of two phase dual-stator motors with both an iron core rotor and ironless rotor. The dual-stator radial-flux PM motor was designated as the DSRF motor and included an iron core rotor, as indicated in Fig. 1(a). The DSRF motor with an ironless rotor was designated as the ironless DSRF motor, as indicated in Fig. 1(b). The proposed

dual-stator axial-flux motor with an ironless rotor was designated as the ironless DSAF motor as indicated in Fig. 1(c). In these motors, each stator contained 16 slots that were purposely equipped with group-concentrated windings [29] to implement the Only-Pull drive technique; the rotor consisted of 18 arc-shaped magnetic poles which were radially or axially magnetized depending on the rotor construction in each motor.

In the DSRF motor, the magnets were fixed on both surfaces of the iron core. The magnet elements were placed in a back-to-back pattern in two layers on both sides of the rotor core such that the magnet elements were magnetized in the opposite polarity elements. The DSRF motor can be regarded as a combination of two separate motors. This arrangement may suffer a significant repulsive force between the mounted PMs that have opposite magnetizing directions and has the risk of demagnetization under extreme conditions. The existence of an iron core in the DSRF motor may contribute additional losses and does not offer the ability to use use dual-stator motors in applications that are either sensitive to the iron core material in the rotor or where the core loss of the rotor is critical. However, an ironless rotor structure overcomes these issues due to the existence of an iron core and single layer of magnets that help to eliminate the risk of repulsive forces and core loss from the rotor. In the ironless DSRF motor and the proposed ironless DSAF motor, the rotor consisted of a single layer of magnet elements; a non-magnetic support was used to fix the magnets without an iron core. The ironless rotor structure offers the ability to use dual-stator motors in the aforementioned applications, such as fixed speed ventilation fans to remove the heat in food processing industries. Moreover, reduction of the cogging torque and the mechanical robustness of rotors with non-magnetic material support can be favorable compared to the rotors with surface glued magnets. The radial-flux configuration illustrates the limitations of obtaining the desired trapezoidal back-EMF waveform for the Only-Pull drive technique. However, an axial-flux configuration was adopted in the proposed motor to obtain the trapezoidal back-EMF waveform. A simple rectangular geometry for the teeth on each stator and axially magnetized magnet poles on the rotor was considered to improve the trapezoidal back-EMF waveform.

B. OPERATION PRINCIPLE

The Only-Pull drive technique controls the motor to operate only during the pull-process, which maintains the magnet health even when higher currents are applied in the stator windings. The push process which is responsible for demagnetization when used in the pull-push drive technique, is avoided when using the Only-Pull drive technique. This drive technique makes the use of higher electrical loading feasible in PM motors without the risk of demagnetization, at the cost of efficiency. However, the DSAF motor with an ironless rotor is focuses on obtaining an effective flux linkage in the windings of both the stators and maximizing the benefit

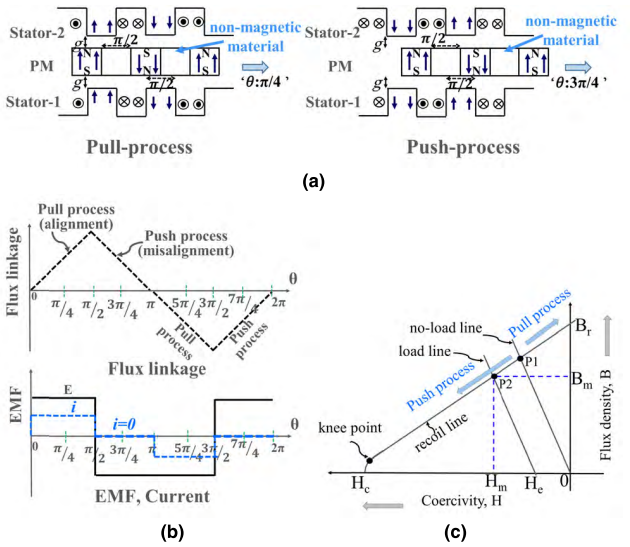

FIGURE 2. Basic concept of pull process and push process for the proposed ironless motor, (a) design layout, (b) flux linkage and EMF, and (c) BH curve.

from the Only-Pull drive technique due to the trapezoidal shape of the back-EMF.

When the rotor is rotated, the magnetic flux linkage changes with respect to the angular position of the rotor. To elaborate this concept, an ideal waveform of the flux linkage and the corresponding EMF were considered. The ideal waveform of the flux linkage is a pure triangular waveform as shown in Fig. 2(a), whereas the ideal waveform of the back-EMF is a pure square waveform, as shown in Fig. 2(b). The basic concept of the pull and push processes of the flux linkage from one stator tooth and one magnet pole is displayed in Fig. 2. Fig. 2(a) illustrates the design layout of the proposed DSAF motor and Fig. 2(b) indicates the corresponding flux linkage, EMF, and phase current in the stator windings for the Only-Pull drive technique. The pull process involves the alignment of the magnet poles with the stator teeth. When the rotor pole begins to align with the stator teeth, until full alignment, the flux linkage increases linearly to the maximum value. This occurs because the direction of the flux flow from the magnet is in the same direction as that of the flux produced by the current in the coil. That means that the north pole of the magnet and the south pole of the coil are supporting the flux distribution.

In a similar fashion, the push process involves the misalignment of the magnet poles with the stator teeth. When a rotor pole leaves the fully aligned position, until there is no overlapping between the poles and the teeth (or misalignment), the net flux linkage decreases linearly to zero. The ratio of the decreasing flux linkage is the same as that of the increasing flux linkage because of the symmetry in the motors. This occurs because of the deterioration in the main flux due to the opposite direction of the flux from the magnet to that of flux from the current in the coil.

These pull and push processes are demonstrated in Fig. 2(c) on the BH curve in the second quadrant. All conventional PM

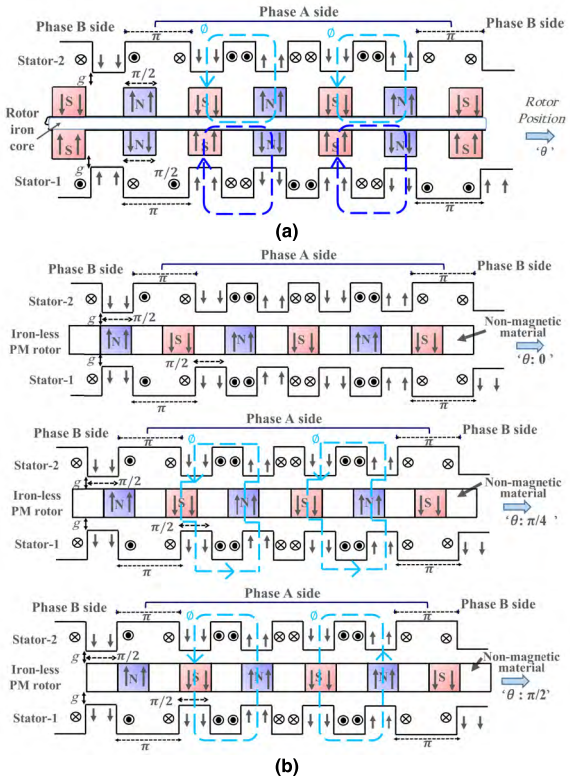

FIGURE 3. Operation principle under no-load and load condition, (a) DSRF motor, (b) ironless DSRF motor and proposed ironless DSAF motor at $\theta = 0$, $\pi/4$, and $\pi/2$ electrical radians.

motors operate by following both the pull process and push process of the pull-push drive technique. In the pull process, the operating point of the magnet moves upwards from the basic point 'P1' of the no-load line. However, the operating point drops to the point 'P2' or towards the knee point in the push process because of the opposite flux.

The no-load operation which produces the back-EMF is defined using the flux linkage and alignment angle of the rotor with the stator teeth by one phase group of both the iron core and ironless motors. The load operation, which produces torque using the Only-Pull drive technique, is explained by the control of current excitation with respect to the flux linkage. Fig. 3 displays the operating principles of the iron core and ironless motors under both no-load and load conditions.

1) NO-LOAD OPERATION

Under no-load conditions, the rotor poles in the presented motors undergo both alignment and misalignment in the absence of current in the windings. In the DSRF motor, two parallel flux loops are formed in two air gaps from both stators as displayed in Fig. 3(a). The main flux flows from one magnet to the teeth of stator-1 through the lower air gap. Following the yoke of stator-1, the flux returns to the opposite polarity magnet and completes the loop back to the first magnet through the rotor iron core. In a similar fashion, the flux completes its loop for stator-2 through the upper air gap. Thus, the flux from the two layers of the magnets flows

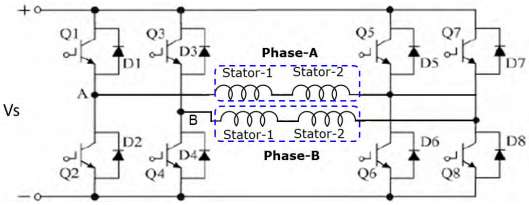

FIGURE 4. Power inverter topology of dual-stator two phase motor using the Only-Pull drive technique.

in the upper and lower airgaps independently. The amount of flux linkage is different in the stators and each stator has its own induced back-EMF.

Fig. 3(b) illustrates the same magnetic circuit for both the ironless DSRF and proposed ironless DSAF motor and indicates the flux path. Three positions of the rotor are displayed ($\theta = 0$, $\pi/4$, and $\pi/2$ electrical radians) that belong to the alignment region of the poles, as indicated in Fig. 2(b). One series flux loop is formed in two air gaps from both stators. The main flux flows from one magnet to the stator-1 tooth through the lower airgap, through the yoke of stator-1, from the adjacent tooth of stator-1 to the opposite polarity magnet, into the stator-2 tooth through the upper air gap, and then completes the loop from the adjacent tooth of stator-2 to the first magnet through the yoke. The flux from the same magnet in a single layer flows both in the upper and lower air gaps and follows the two air gaps in series. An equal flux linkage is experienced by the windings in both stators. Consequently, the induced back-EMF of the stators is dependent on the same layer of the magnets.

2) LOAD OPERATION

Under load conditions, the DSRF, ironless DSRF, and proposed ironless DSAF PM motors are driven by the Only-Pull drive technique. The control of current excitation for these motors is similar and based on phase conduction of $\pi/2$ electrical radians. The current is injected during alignment from $\theta = 0$ to $\pi/2$ electrical radians and maintained at zero for the misalignment of the rotor poles with the teeth of the stator. The positions of the rotor during this alignment are the same as indicated in Fig. 3(b).

Control of the proposed two-phase motor for the Only-Pull drive technique is provided by the power inverter topology displayed in Fig. 4. The inverter consists of 4-legs with eight switches (Q1-Q8). Four switches (Q1, Q2, Q5, and Q6) conduct for phase-A and the other four switches (Q2, Q4, Q7, and Q8) conduct during phase-B. The sequence of gating signals is 1001 and 0110 to generate a pulse of positive current and negative current for phase-A and phase-B, respectively. The inverter current is applied to both positive and negative regions of the pull process until the magnet poles fully align with the teeth of each stator within one phase (e.g., phase-A) for $\pi/2$ electrical radians. In the next commutation, the windings of phase-B are excited for the alignment of the next two groups of four magnet poles. This process utilizes half of the back-EMF corresponding to only the pull process

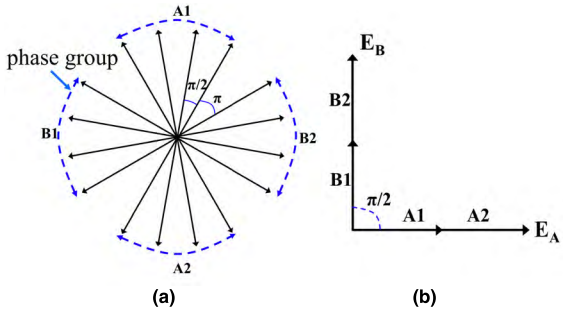

FIGURE 5. Group-concentrated windings used to implement the Only-Pull drive technique, (a) star of stator coils, (b) resultant EMF vector.

flux and produces torque via the conduction of two phases, each phase from one stator. In the DSRF motor, the magnet poles from the lower layer affect only the alignment with the teeth of stator-1; the magnet poles from the upper layer on the rotor affect only the alignment with the teeth of stator-2; leading to a net torque production. Alternatively, in the ironless DSRF and ironless DSAF motors, each magnet element affects the alignment with the teeth of both stator-1 and stator-2 simultaneously. Thus, the ironless motors are expected to deliver a similar torque utilizing almost half of the magnet volume compared to the DSRF motor.

C. DESIGN CONCEPT

The design of the two phase dual-stator motor is conducted based on the Only-Pull process technique. The selection of stator slots and rotor magnet poles for the two phase motor is given by (1)

$$2p = 2 * n_1 * n_2 + n_2 \tag{1}$$

where n_1 is the number of coils for one phase group and n_2 is the number of groups for one phase.

A series of motors can be designed with different combinations of n_1 and n_2. In this paper, the motors were furnished with 16 slots and 18 poles (16S18P) to minimize the volume of one magnet pole for the Only-Pull drive technique. Each stator had a group-concentrated winding configuration. This configuration facilitates the control of the alignment of the magnet poles with the stator teeth by controlling the phase current independently. In this configuration, adjacent coils are wound with opposite polarity to form the phase groups (e.g., A1, A2) as indicated in Fig. 5(a). Each phase group of one phase was physically and electrically isolated from the phase groups of another phase. The induced EMF of these coils within the group follows the same direction resulting in the largest EMF vector as indicated in Fig. 5(b). An additional slot width of $\pi/2$ electrical radians between each phase group of phase-A and phase-B was designed to produce symmetry in the back-EMF.

Because of the cylindrical configuration of the radial-flux and disc configuration of the axial-flux motor, the flux per pole is proportional to the air-gap diameter in the DSRF and ironless DSRF motors, whereas, the flux per pole is proportional to the square of the outer diameter of the disc

TABLE 1. Specifications of the investigated models.

Metrics	Units	DSRF	Ironless DSRF	Ironless DSAF
Slots/poles	-	16/18	16/18	16/18
Rated speed	rpm	1580	1580	1580
Magnet thickness	mm	1.5×2	1.5	2
Air gap length	mm	0.9×2	0.9×2	0.9×2
Turns per phase	-	80	80	152
NdFeB Magnet Br / Hc	T, kA/m	1.2 / 940	1.2 / 940	1.2 / 940
Outer air gap radius	mm	39	39	-
Inner air gap radius	mm	33.5	36.8	-
Inner radius of stator/rotor	mm	-	-	50.5
Outer radius of stator/rotor	mm	-	-	97
Stator yoke thickness (stator-1/stator-2)	mm	7.4/10.1	7.4/10.1	7.5/7.5
Iron volume	mm^3	517503	514437	409132
Copper volume	mm^3	65159	65159	63969
Magnet volume	L	0.031	0.016	0.014

in the proposed DSAF motor. Therefore, the main dimensions of the DSRF and ironless DSRF motors were determined using the D^2L sizing method [30], whereas, the main dimensions of ironless DSAF motor were extracted using the D^3 sizing method [31] by equating the magnetic flux per pole with that of the ironless DSRF motor. Table 1 lists the specifications of all three models. The design features of the ironless DSRF and DSAF models compared to those of the DSRF motors are as follows:

- In the DSRF motor, the magnets were mounted on both sides of the rotor.
- In the ironless motors, a non-magnetic steel holder could be used to fix the magnets.
- The ironless DSAF motor was designed based on the criteria of an equal airgap flux per pole as in the ironless DSRF motor.
- The electrical loading was maintained equal for both stators in the three motors.
- By utilizing the ironless rotor, only half of the magnet volume was used compared to that of the DSRF motor.

III. PERFORMANCE EVALUATION USING FEA

The performance characteristics of dual-stator motors with an iron core and ironless rotors were evaluated using ANSOFT finite element software. The motors were analyzed under both no-load and load conditions. The no-load flux density in each airgap, flux linkage, back-EMF, and output torque were illustrated to indicate the comparison of each topology using the Only-Pull drive technique.

A. FLUX DENSITY

The air-gap flux density in the DSRF and ironless DSRF motors was obtained on the mean radius determined by the outer radius of the rotor and inner radius of the stator, and the air-gap flux density in the DSAF motor was obtained on the mean radius determined by the inner radius and outer

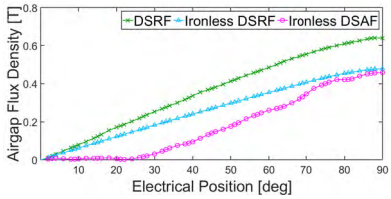

FIGURE 6. Comparison of flux density in upper air gap versus position during only pull process.

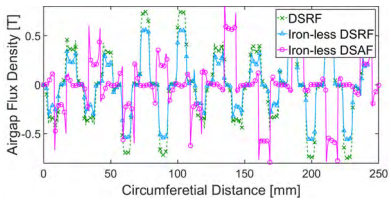

FIGURE 7. Comparison of air gap flux density in upper air gap versus circumferential distance.

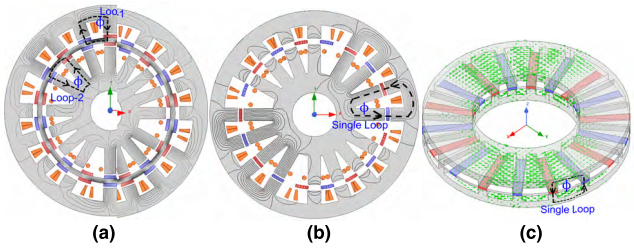

FIGURE 8. Distribution of magnetic flux of dual-stator PM motors, (a) parallel circuit: DSRF model, (b) series circuit: ironless DSRF model, and (c) series circuit: ironless DSAF model.

radius of the stator or rotor. Fig. 6 illustrates the no-load airgap flux density variation in the upper air gap with respect to the angular position from the beginning of alignment to full alignment of the magnet poles with the stator teeth during the Only-Pull process for the DSRF and ironless DSRF motors. The larger magnetic equivalent air gap in the ironless motors, because of the ironless rotor structure, results in lower flux density values compared to iron core motor, which affects the amount of the induced back-EMF.

Fig. 7 depicts the no-load airgap flux density in the upper air gap along the circumference. The magnets threw the flux into the air gap for a span of $\pi/2$ electrical radians. Each air gap flux predicted the back-EMF in the phase of the corresponding stator. In the DSRF motor, the volume of the magnet element on the lower layer was less than that of the upper layer magnet elements because of the smaller inner radius. The flux density in the lower airgap is comparatively less than that in the upper air gap. Conversely, in the ironless DSRF and ironless DSAF motors, the flux density in the two airgaps was similar. The span of the air gap flux density described the maximum possible alignment of the magnet with the stator teeth in the pull process for the specified operation of the motor. The distribution of the magnetic flux for the motors is displayed in Fig. 8. This magnetic flux distribution confirmed the formation of the parallel and series magnetic circuits in

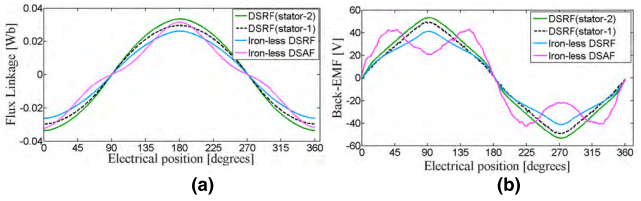

FIGURE 9. Comparison of (a) flux linkage of upper and lower stator winding and, (b) Back-EMF in each stator windings.

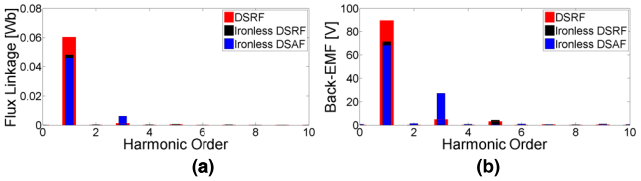

FIGURE 10. FFT comparison of (a) flux linkage, (b) back-EMF.

the motors. As expected, in the DSRF motor, the flux flowed in two airgaps independently. Alternatively, in the ironless DSRF and ironless DSAF motors, the flux flowed in the two airgaps mutually.

B. FLUX LINKAGE, AND BACK-EMF

Fig. 9(a) illustrates the flux linkage for these motors. The difference in the flux linkage of the two stators in the DSRF motor was caused by the different flux density in the two air gaps. This occured because of the relatively small span of the magnet elements on the smaller radius at the lower air gap. Therefore, a different amount of back-EMF was induced in the two stators. Conversely, in the ironless DSRF motor, an equal amount of flux was linked in the two stators. Consequently, an equal amount of back-EMF was induced in both stators as indicated in Fig. 9(b). However, the equivalent airgap formed by both the magnets and physical airgap length was large in the ironless DSRF motor, which caused a reduction in the back-EMF. The ironless DSAF motor containing the rectangular stator teeth and magnet poles provided an equal flux linkage and produced a back-EMF that is comparable to that of the ironless DSRF motor. A fast Fourier transform (FFT) was performed for the combined flux linkage from both the stators, and the corresponding back-EMF of the motors as shown in Fig. 10(a) and (b), respectively. The magnitude of the fundamental component of both the flux linkage and the back-EMF was larger for the DSRF motor, however, the magnitude of the third order harmonic component was significantly larger for the ironless DSAF motor, which produced a trapezoidal back-EMF because the flux linkage was more linear in the DSAF motor.

C. COGGING TORQUE, AVERAGE TORQUE, AND EFFICIENCY

The cogging torque caused by the interaction between the magnets and stator teeth [29] was compared using the iron core rotor and ironless rotor. The DSRF motor demonstrated a higher cogging torque, whereas, the ironless motors indicated

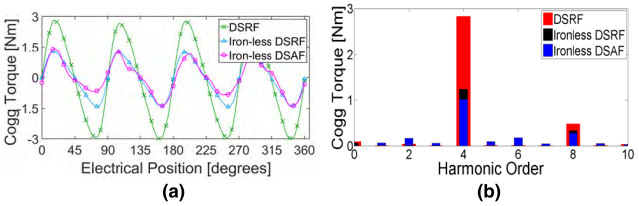

FIGURE 11. Comparison of (a) cogging torque showing the cogging period, and (b) FFT of the cogging torque.

TABLE 2. Comparison of results for iron core rotor and ironless rotor motors.

Metrics	Units	DSRF	Ironless DSRF	Ironless DSAF
Back-EMF (inner/ outer)	V	31.9/28.4	23.8/23.8	26.5/26.5
Average torque	Nm	2.7	2.3	2.74
Winding current	A	6.6	6.6	6.6
Torque per magnet volume	Nm/L	87	143.7	195.7
Cogging torque, pk2pk	Nm	5.8	2.8	2.8
Torque ripple	%	537	370	182
Copper loss	W	150	150	150
Iron loss	W	91.50	90.92	72.31
Total losses	W	252.67	250.43	233.64
Efficiency	%	63.87	60.31	66.0

a reduction in the cogging torque as shown in Fig. 11(a), and the values are compared in Table 2. The results indicate that the proposed ironless motor had a significant reduction in the cogging torque despite having aligned stators.

The cogging torque period, $\theta_{cog-period}$, of the motors can be calculated by (2), which gives the values of 10 mechanical degrees or 90 electrical degrees and shows four cycles in 360 electrical degrees

$$\theta_{cog-period} = 360°/lcm(N_s, 2p) * n_1, \tag{2}$$

where N_s, $2p, n_1$ and lcm represent the number of slots, number of poles, the number of slots per phase group, and the least common multiple, respectively. The frequency of the cogging cycles was also confirmed by analyzing the FFT of the cogging torque waveform, as shown in Fig. 11(b), which confirms the four cycles in 360 electrical degrees.

The motors were driven by the Only-Pull drive technique at a rated RMS current of 6.6 A that produced a higher current density of 13.2 A/mm^2 that was inherently due to the use of thin magnets. The harmonic components in the back-EMF waveform corresponding to the identical harmonic components present in the square waveform of the current shown in Fig. 12, contributed additional torque. Here, the third order harmonic component was responsible for major part of this additional torque in the case of the ironless DSAF motor. Fig. 13(a) depicts a transient waveform of the electromagnetic torque and Fig. 13(b) depicts a comparison of average values of the torque based on the Only-Pull drive technique for all models. Table 2 lists these values based on similar

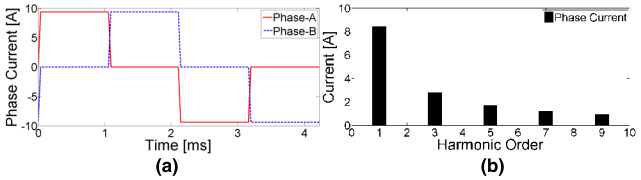

FIGURE 12. Current applied for the Only-Pull drive technique (a) phase current, and (b) FFT of phase current.

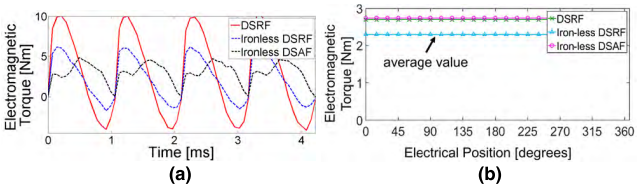

FIGURE 13. Comparison of electromagnetic torque using Only-Pull drive technique (a) transient waveform, (b) showing the average value of the torque.

electric loadings. The influence of the equivalent air gap and harmonic components is clear with the distinction of the average torque. The ironless DSAF motor produced an equal torque of 2.74 Nm and utilized half of the magnet volume compared to the DSRF motor. The comparison revealed that the torque per magnet volume for both ironless models is significantly higher than that of the DSRF model.

To calculate the efficiency, the iron losses P_{iron}, in the core of the motor, and copper losses P_{cu}, from the stator windings were considered. The iron losses for POSCO steel material 50PN470 (s18) were obtained from the data sheet given by the manufacturer. However, the copper losses in the two stators can be obtained by (3)

$$P_{cu} = 2 \times m \times I_{rms}^2 \times R_{ph}, \tag{3}$$

where m is the number of phases, I_{rms} is the RMS value of the phase current, and R_{ph} is the stator winding phase resistance. The iron losses and copper losses for each motor are listed in Table 2. The values of the copper losses are higher because of the higher current density in the motor which affects the efficiency of the motor. The stray and mechanical losses were assumed to be 2.5% of output power. The efficiency of the motors was estimated by (4)

$$\eta = P_{out}/(P_{out} + P_{cu} + P_{iron}) \times 100, \tag{4}$$

A comparison of the efficiency of the motors is presented in Table 2. The DSRF motor exhibited an efficiency of 63.87%, the efficiency of the ironless DSRF motor was 60.31%, and that of the proposed ironless DSAF motor was 66%. The results reveal that the proposed DSAF motor has improved efficiency, because of higher average torque and torque per magnet volume even though utilizes half the magnet volume compared to the DSRF motor.

When considering the abnormal condition where the windings of one stator are disconnected, the ironless DSAF motor can still provide better torque per magnet volume and

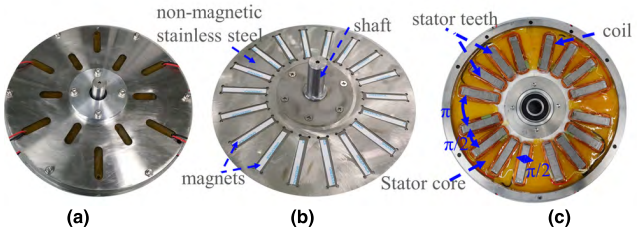

FIGURE 14. Prototype of the proposed ironless DSAF motor, (a) complete assembly of the motor, (b) rotor with magnet poles and non-magnetic structure, and (c) stator with group-concentrated windings.

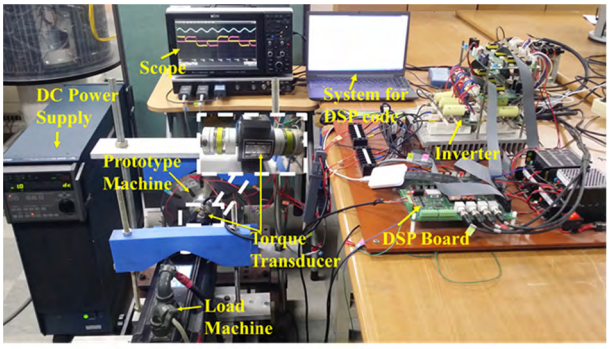

FIGURE 15. Test bed for the ironless DSAF motor.

the path of flux in the stators will be the same. However, in the case of a short circuit fault between the windings of two phases, the behavior of the machine changes and the flux may be disturbed.

IV. EXPERIMENTAL VALIDATION

A. EXPERIMENTAL SETUP

Based on the merits of the ironless dual-stator axial-flux motor, a prototype was built to test and validate the FEA results. Each component of the prototype is presented in Fig. 15. Fig. 14(a) displays the complete assembly of the motor. Fig. 14(b) displays an ironless rotor, where the magnet poles are fixed with a non-magnetic stainless steel SUS304 material. The installation of the PMs during the manufacture of the prototype was challenging. The non-magnetic stainless steel structure was carefully designed to hold the PMs in their specified angular position, keep the uniform air gap around the circumference, and fulfill the criteria of implementing the Only-Pull drive technique. Because both the stators were the same, only one is shown in Fig. 14(c). The stator slots were equipped with group-concentrated winding with an additional slot width between the two phase groups to produce a balanced back-EMF in the phases. The testbed is presented in Fig. 15 with a prototype machine connected to the load machine, inverter drive, digital signal processing (DSP) board, oscilloscopes, and DC power supply. A commercial torque transducer (SETTech) was used to measure the torque during the experiment.

B. EXPERIMENTAL RESULTS AND DISCUSSION

Under the no-load condition, the motor was tested to confirm the back-EMF profile by rotating the shaft via a prime mover

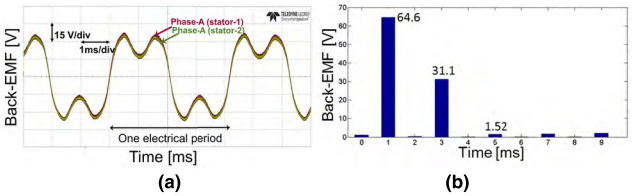

FIGURE 16. No-load results for the ironless DSAF motor prototype (a) back-EMF and, (b) FFT of the measured back-EMF.

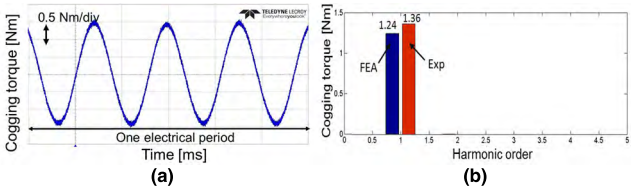

FIGURE 17. Cogging torque of the ironless DSAF motor prototype (a) measured waveform showing the cogging period and, (b) comparison of the fundamental component of the cogging torque using FEA and experiment.

TABLE 3. Comparison of results from simulation and prototype test.

Metric	Units	Simulation	Prototype
Back-EMF, E_{rms}	V	53	52.48
Average torque	Nm	2.74	2.66
Cogging torque, pk2pk	Nm	2.8	2.98
Torque per magnet volume	Nm/L	195.7	189.6
Torque ripples	%	182	206.2
Efficiency	%	66.0	65.4

motor at the rated speed. Fig. 16(a) depicts the measured back-EMF induced in one phase windings of two stators; these are listed in Table 3. The measured result verified the trapezoidal back-EMF for the axial-flux configuration of the proposed motor obtained using the simulation in Fig. 9. The FFT of measured back-EMF of the series-connected stators is shown in Fig. 16(b), which confirms the larger magnitude of the third order harmonic in the waveform. Moreover, the exact same back-EMF in each stator was obtained because of the equal flux linkage from the ironless rotor with a single layer of magnets. The RMS value of the back-EMF from the experiment was 52.48 V, close to the 53 V from the simulation, shown in Fig. 9(b). The cogging torque of the prototype motor was measured under the no-load condition and is illustrated in Fig. 17(a), and the FFT over one cycle of the cogging torque was obtained from FEA and the compared with the experimental results in Fig. 17(b). The measured value of the peak-to-peak cogging torque was 2.98 Nm verifying the cogging torque reduction in the proposed DSAF motor with an ironless rotor structure. It was observed that the measured results are in agreement with the simulation results, shown in Fig. 11(a).

Furthermore, the torque output was verified under the load condition by connecting both the stators in series for convenience. The rotor position was obtained using a rotary encoder at the rated speed. A closed-loop current controller

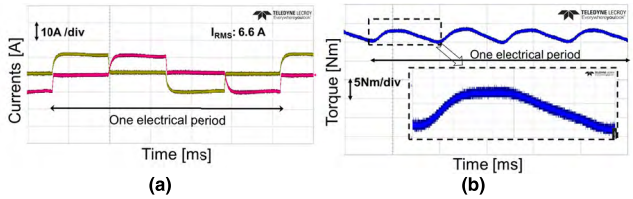

FIGURE 18. Load results of the ironless DSAF motor prototype, (a) phase currents and, (b) electromagnetic torque.

was employed to the power inverter displayed in Fig. 4 to control the magnitude and position of the phase currents for implementing the Only-Pull drive technique. The supplied phase currents and measured output torque are depicted in Fig. 18(a) and (b), respectively. The average torque of 2.66 Nm was also in close agreement with the simulation result of 2.74 Nm, given in Fig. 13(b); a comparable torque per magnet volume was also found. Similarly, the efficiency of the prototype was calculated based on the average torque measured from the experiment and the losses were assumed to be equal to the losses obtained from the material data sheet given in Table 3. The efficiency comparison was satisfactory and maintained even when utilizinghalf the magnet volume compared to that of the DSRF motor.

V. CONCLUSION

In this paper, a two phase dual-stator axial-flux (DSAF) permanent magnet BLDC motor with an ironless rotor structure and driven by an Only-Pull drive technique, was proposed. The design and topology of the proposed DSAF PM motor were validated by no-load and full-load experimental results of a prototype using the Only-Pull drive technique. A greater torque per magnet volume of the proposed ironless DSAF motor was achieved whilst utilizing only half the magnet volume and keeping the same electrical loading. Furthermore, the efficiency was maintained and the cogging torque was significantly reduced compared to the DSRF iron rotor motor. As a result, the dual-stator axial-flux motor with an ironless rotor would appear to be an effective and economical solution for the Only-Pull drive technique, saving magnet volume and the overall cost of the motor without demagnetization.

REFERENCES

[1] Q. Wang, S. Niu, and L. Yang, "Design optimization and comparative study of novel dual-PM excited machines," *IEEE Trans. Ind. Electron.*, vol. 64, no. 12, pp. 9924–9933, Dec. 2017.

[2] D. Zhang, K. T. Chau, S. Niu, and J. Z. Jiang, "Design and analysis of a double-stator cup-rotor PM integrated-starter-generator," in *Proc. IEEE 41st Annu. Meeting Rec. Ind. Appl. Conf. (IAS)*, Tampa, FL, USA, Oct. 2006, pp. 20–26.

[3] R. N. F. K. R. Othman, N. A. M. Zuki, S. R. C. Ahmad, F. A. A. Shukor, and S. Z. M. Isa, M. N. Othman, "Modelling of torque and speed characterisation of double stator slotted rotor brushless DC motor," *IET Electr. Power Appl.*, vol. 12, no. 1, pp. 106–113, 2018.

[4] C. Feng, X. Jing, G. Bin, C. Shukang, and Z. Jiange, "Double-stator permanent magnet synchronous in-wheel motor for hybrid electric drive system," *IEEE Trans. Magn.*, vol. 45, no. 1, pp. 278–281, Jan. 2009.

[5] Y. Wang, M. Cheng, Y. Du, and K. T. Chau, "Design of high-torque-density double-stator permanent magnet brushless motors," *IET Electr. Power Appl.*, vol. 5, no. 3, pp. 317–323, Mar. 2011.

[6] A. Mlot, A. C. Malloy, and M. Lampérth, "Effect of rotor/stator misalignment on the performance of a permanent magnet axial-flux motor," in *Proc. 8th IET Int. Conf. Power Electron., Mach. Drives (PEMD)*, Glasgow, U.K., 2016, p. 6.

[7] W. Zhao, T. A. Lipo, and B.-I. Kwon, "Comparative study on novel dual stator radial flux and axial flux permanent magnet motors with ferrite magnets for traction application," *IEEE Trans. Magn.*, vol. 50, no. 11, Nov. 2014, Art. no. 8104404.

[8] S. Niu, K. T. Chau, and C. Yu, "Quantitative comparison of double-stator and traditional permanent magnet brushless machines," *J. Appl. Phys.*, vol. 105, no. 7, 2009, Art. no. 07F105.

[9] S. Niu, K. T. Chau, J. Z. Jiang, and C. Liu, "Design and control of a new double-stator cup-rotor permanent-magnet machine for wind power generation," *IEEE Trans. Magn.*, vol. 43, no. 6, pp. 2501–2503, Jun. 2007.

[10] X. Liu, H. Lin, Z. Q. Zhu, C. Yang, S. Fang, and J. Guo, "A novel dual-stator hybrid excited synchronous wind generator," *IEEE Trans. Ind. Appl.*, vol. 45, no. 3, pp. 947–953, May 2009.

[11] F. Chai, S. Cui, and S. Cheng, "Performance analysis of double-stator starter generator for the hybrid electric vehicle," *IEEE Trans. Magn.*, vol. 41, no. 1, pp. 484–487, Jan. 2005.

[12] X. Huang, K. Zhang, L. Wu, Y. Fang, and Q. Lu, "Design of a dual-stator superconducting permanent magnet wind power generator with different rotor configuration," *IEEE Trans. Magn.*, vol. 53, no. 6, Jun. 2017, Art. no. 8700204.

[13] J. Zheng, W. Zhao, J. Ji, J. Zhu, C. Gu, and S. Zhu, "Design to reduce rotor losses in fault-tolerant permanent-magnet machines," *IEEE Trans. Ind. Electron.*, vol. 65, no. 11, pp. 8476–8487, Nov. 2018.

[14] S. S. Nair, V. I. Patel, and J. Wang, "Post-demagnetization performance assessment for interior permanent magnet AC machines," *IEEE Trans. Magn.*, vol. 52, no. 4, Apr. 2016, Art. no. 8102810.

[15] T. Raminosoa, C. Gerada, N. Othman, and L. D. Lillo, "Rotor losses in fault-tolerant permanent magnet synchronous machines," *IET Electr. Power Appl.*, vol. 5, no. 1, pp. 75–88, 2011.

[16] B. A. Welchko, T. M. Jahns, W. L. Soong, and J. M. Nagashima, "IPM synchronous machine drive response to symmetrical and asymmetrical short circuit faults," *IEEE Trans. Energy Convers.*, vol. 18, no. 2, pp. 291–298, Jun. 2003.

[17] G. Choi and T. M. Jahns, "Interior permanent magnet synchronous machine rotor demagnetization characteristics under fault conditions," in *Proc. IEEE Energy Convers. Congr. Expo. (ECCE)*, Sep. 2013, pp. 2500–2507.

[18] G.-H. Kang, J. Hur, H. Nam, J.-P. Hong, and G.-T. Kim, "Analysis of irreversible magnet demagnetization in line-start motors based on the finite-element method," *IEEE Trans. Magn.*, vol. 39, no. 3, pp. 1488–1491, May 2003.

[19] P. Sergeant and A. P. M. Van den Bossche, "Influence of the amount of permanent-magnet material in fractional-slot permanent-magnet synchronous machines," *IEEE Trans. Ind. Electron.*, vol. 61, no. 9, pp. 4979–4989, Sep. 2014.

[20] I. Petrov, M. Niemelä, P. Ponomarev, and J. Pyrhönen, "Rotor surface ferrite permanent magnets in electrical machines: Advantages and limitations," *IEEE Trans. Ind. Electron.*, vol. 64, no. 7, pp. 5314–5322, Jul. 2017.

[21] P. Peng, H. Xiong, J. Zhang, W. Li, F. Leonardi, C. Rong, M. W. Degner, F. Liang, and L. Zhu, "Effects of external field orientation on permanent magnet demagnetization," *IEEE Trans. Ind. Appl.*, vol. 53, no. 4, pp. 3438–3446, Jul./Aug. 2017.

[22] J.-X. Shen, P. Li, M.-J. Jin, and G. Yang, "Investigation and countermeasures for demagnetization in line start permanent magnet synchronous motors," *IEEE Trans. Magn.*, vol. 49, no. 7, pp. 4068–4071, Jul. 2013.

[23] K.-Y. Hwang, B.-Y. Yang, S.-H. Rhyu, B.-T. Kim, D.-K. Kim, S.-B. Rhee, and B.-I. Kwon, "Optimal rotor design for reducing the partial demagnetization effect and cogging torque in spoke type PM motor," *J. Appl. Phys.*, vol. 105, no. 7, 2009, Art. no. 07F123.

[24] L. Alberti, E. Fornasiero, and N. Bianchi, "Impact of the rotor yoke geometry on rotor losses in permanent-magnet machines," *IEEE Trans. Ind. Appl.*, vol. 48, no. 1, pp. 98–105, Jan./Feb. 2012.

[25] A. M. El-Refaie, "Fractional-slot concentrated-windings synchronous permanent magnet machines: Opportunities and challenges," *IEEE Trans. Ind. Electron.*, vol. 57, no. 1, pp. 107–121, Jan. 2010.

[26] N. Bianchi, M. Pré, G. Grezzani, and S. Bolognani, "Design considerations on fractional-slot fault-tolerant synchronous motors," in *Proc. IEEE Int. Conf. Electr. Mach. Drives*, May 2005, pp. 902–909.
[27] T. Yazdan, W. Zhao, T. A. Lipo, and B. I. Kwon, "A novel technique for two-phase BLDC motor to avoid demagnetization," *IEEE Trans. Magn.*, vol. 52, no. 7, Jul. 2016, Art. no. 8106704.
[28] T. Yazdan and B.-I. Kwon, "Electromagnetic design and performance analysis of a two-phase AFPM BLDC motor for the only-pull drive technique," *IET Electr. Power Appl.*, vol. 12, no. 7, pp. 999–1005, Aug. 2018.
[29] M. Aydin and M. Gulec, "Reduction of cogging torque in double-rotor axial-flux permanent-magnet disk motors: A review of cost-effective magnet-skewing techniques with experimental verification," *IEEE Trans. Ind. Electron.*, vol. 61, no. 9, pp. 5025–5034, Sep. 2014.
[30] S. Huang, J. Luo, F. Leonardi, and T. A. Lipo, "A general approach to sizing and power density equations for comparison of electrical machines," *IEEE Trans. Ind. Appl.*, vol. 34, no. 1, pp. 92–97, Jan./Feb. 1998.
[31] S. Huang, J. Luo, F. Leonardi, and T. A. Lipo, "A comparison of power density for axial flux machines based on general purpose sizing equations," *IEEE Trans. Energy Convers.*, vol. 14, no. 2, pp. 185–192, Jun. 1999.

TANVEER YAZDAN was born in 1989. He received the B.Sc. degree in electrical engineering from the University of Engineering and Technology Taxila, Pakistan, in 2010, and the M.S. and Ph.D. degrees in electrical engineering from Hanyang University, South Korea, in 2018. From 2010 to 2013, he was an Assistant Manager with Karachi-Electric Company, Pakistan. He is currently an Assistant Professor with The University of Lahore, Pakistan. His research interest includes design and control of electric machines.

SHAHID ATIQ was born in Punjab, Pakistan. He received the bachelor's and master's degrees from the University of Engineering and Technology Taxila, Pakistan, and the Ph.D. degree from the Energy Conversion Systems Laboratory, Hanyang University, South Korea. He held different managerial and educational positions at various institutions. He is currently an Associate Professor and the Head of the Electrical Engineering Department, Khwaja Fareed University of Engineering & Information Technology, Rahim Yar Khan, Pakistan.

BYUNG-IL KWON was born in 1956. He received the B.S. and M.S. degrees in electrical engineering from Hanyang University, Ansan, South Korea, in 1981 and 1983, respectively, and the Ph.D. degree in electrical engineering and machine analysis from The University of Tokyo, Tokyo, Japan, in 1989. From 1989 to 2000, he was a Visiting Researcher with the Faculty of Science and Engineering, University of Waseda, Tokyo. In 1990, he was a Researcher with the Toshiba System Laboratory, Yokohama, Japan. In 1991, he was a Senior Researcher with the Institute of Machinery and Materials Magnetic Train Business, Daejeon, South Korea. From 2001 to 2008, he was a Visiting Professor with the University of Wisconsin–Madison, Madison, WI, USA. He is currently a Professor with Hanyang University. His research interest includes design and control of electric machines.

NOMAN BALOCH was born in 1987. He received the B.S. degree in electronics engineering from the Balochistan University of Information Technology, Engineering and Management Sciences (BUITEMS), Quetta, Pakistan, in 2010. He is currently pursuing the M.S. and Ph.D. degrees with the Department of Electronics System Engineering, Hanyang University, Ansan, South Korea.

From 2010 to 2015, he was a Deputy Assistant Director with the National Database and Registration Authority (NADRA), Pakistan. His research interest includes design and control of electrical machines.

JUNG-WOO KWON was born in 1992. He received the B.S. degree in bio-nano engineering and electrical engineering from Hanyang University, Ansan, South Korea, in 2015, where he is currently pursuing the M.S. and Ph.D. degrees with the Department of Electronics System Engineering, Hanyang University. His research interest includes electric machines, especially on motors.